CLEAN Progress Report TV III.2: Geomodeling and Process Simulation

Report Period: 01/2009 – 12/2009

U.-J. Görke[1], R. Liedl[2], O. Kolditz[1,2] (Eds.)

contributed by

K.N. Awemo[3], S. Bauer[4], N. Böttcher[2], M. De Lucia[5], L. Ganzer[6]
Y. Gou[6], M.Z. Hou[3,6], M. Kühn[5], R. Meyer[7], C.-H. Park[1]
K. Prokoph[7], E. Ribbe[7], G. Rosenthal[7], C. Schreyer[7], A.K. Singh[1]
L. Stecken[7], M. Tantow[7], G. Voigtländer[7], W. Wang[1], N. Watanabe[1]
J. Yoon[3]

[1] *Helmholtz-Zentrum für Umweltforschung – UFZ, Leipzig,*
[2] *Technische Universität Dresden,*
[3] *Energie-Forschungszentrum Niedersachsen, Goslar*
[4] *Christian-Albrechts-Universität Kiel,*
[5] *GFZ Deutsches Forschungszentrum für Geowissenschaften, Potsdam,*
[6] *Institut für Erdöl- und Erdgastechnik, TU Clausthal,*
[7] *GDF SUEZ E&P Deutschland GmbH*

Abstract

Within the context of the project TV III.2 "Geomodeling and Process Simulation" as a part of the thematic complex "Geoscientific Process Description" methods and numerical tools will be developed which are dedicated to the modeling of the reservoir under consideration as well as the simulation of the processes during CO_2 injection and storage. Consequently, the studies are focussed on the thermodynamic flow simulation in the borehole (TV III.2.1), the analysis of the coupled thermo-hydro-mechanical-chemical processes in the reservoir near-field (TV III.2.2), and the assessment of safety and EGR capabilities of the Altensalzwedel site during CO_2 injection (TV III.2.3). The report summarizes results of the subprojects as parts of an integrated multiscale approach.

TV III.2.2: A systematic for CO_2 benchmarking

Olaf Kolditz[1,2], Norbert Böttcher[3], Ashok Kumar Singh[1], Wenqing Wang[1], Chan-Hee Park[1], Rudolf Liedl[3], Uwe-Jens Görke[1]

[1] *Helmholtz-Zentrum für Umweltforschung – UFZ, Leipzig,*
[2] *Institut für Umweltsystemanalyse, Technische Universität Dresden,*
[3] *Institut für Grundwassermanagment, Technische Universität Dresden*

Abstract

In this report, the current state of benchmarking for numerical methods related to the simulation of CO_2 injection and storage within the CLEAN TV III.2 is reported. Benchmarks are neccesary tools to varify the algorithms and the software dedicated to simulate the separated and differently coupled thermo-hydro-mechanical-chemical (THMC) processes in the subsurface. Process- as well as site-related benchmarks are discussed. The are aimed to serve as common basis for code intercomparison of the different scientific and commercial software used by CLEAN partners.

1 Aims and Goals

Benchmarking of process simulation is one of the cross-cutting activities within the CLEAN TV III.2 "Geomodeling and Process Simulation". This initiative includes a systematic development of appropriate test cases for CO_2 injection and storage as well as the verification procedure itself. The verification methods relies on both classic test cases and inter-code comparison (see, e.g., [2]. The benchmarking strategy comprises three aspects:

- Process-based: Numerical analysis of individual and coupled processes related to CO_2 injection and storage with increasing complexity, i.e. compressible flow (H), two-phase flow (H^2), consolidation (H^2M), thermo-mechanics (TM) up to nonisothermal two-phase flow consolidation (TH^2M processes).
- Thermodynamics-based: Increasing complexity of material behavior, i.e. from constant to highly nonlinear material functions.
- Scenario-based: Development of site-specific test cases (application benchmarks).

Two workshops have been held in 2009 in Leipzig and in Stuttgart concerning the cross-cutting benchmarking activities within the CLEAN project.

2 Methods

In this section we provide an overview on the current available CO_2 benchmark tests. Most of them are described in more detail in the cited literature and OpenGeoSys (OGS) Developer-Benchmark-Book (OGS-DBB 4.10 [4]). The OGS-DBB is an open access online publication available through `www.opengeosys.net`.

The benchmarks are organized by three criteria: processes, thermodynamic properties and storage scenarios.

2.1 Process-based

The systematic of benchmarks by processes is given in Tab. 1. We start from the flow processes, then include mechanical effects (consolidation) and finally consider nonisothermal phenomena (heat transport and phase changes). Chemical reactions are not yet incorporated into this benchmark systematic. OGS is able to handle reactive transport by several build-in chemical simulators such as PHREEQC, ChemApp, BRNS and GEMS (cf. [1,5,6]).

Table 1
Benchmarks by processes.

Problem type	Process type	Dimension	DBB
Compressible flow	H		
Two-phase flow	H^2	1-D Buckley-Leverett	19.3
Two-phase flow	H^2	1-D Mc-Worther	19.4
Two-phase flow	H^2	2-D Keuper	19.5
Unsaturated consolidation	HM	2-D	13.3
Two-phase flow consolidation	H^2M	2-D	13.4
Thermo-mechanics	TM	2-D / 3-D	14
Nonisothermal compressible flow	TH	1-D	
Nonisothermal two-phase flow	TH^2	1-D	
Nonisothermal unsaturated consolidation	THM	2-D	
Nonisothermal two-phase flow consolidation	TH^2M	2-D	

2.2 Thermodynamics-based

The systematic of benchmarks by thermodynamic properties is given in Tab. 1. Complex thermodynamic properties for a variety of relevant fluids have been introduced and implemented in OGS by Böttcher and Liedl (see TV III.2.2-3, this report). Fluid property functions in terms of equations of state (EOS) are described in more detail in the OGS-DBB, Sec. 4.

Table 2
Benchmarks by thermodynamic properties.

Problem type	Acronym	DBB
Redlich-Kwong	RKEOS	4.3.1
Peng-Robinson	PREOS	4.3.2
Helmholtz free energy	HFE	4.3.3

The following fluid properties have been considered: density ρ, enthalpy h, entropy s, heat capacity c_p, visosity μ, thermal conductivity λ. Examples how to use these EOS are given in the OGS-DBB (Sec. 4.2). The following benchmarks for testing the EOS implementation have been investigated:

- CO_2 flow with pressure dependent density and viscosity (nonlinear H process),
- nonisothermal single phase fluid flow (CO_2, CH_4, H_2O, N_2) with variable fluid properties (nonlinear HT process),
- nonisothermal two-phase fluid flow (CO_2, CH_4) with variable fluid properties (nonlinear HT process).

2.3 Scenario-based

The third classification is denoted as scenario-or-site-based (cf. Tab. 3). Ketzin is based on the corresponding site, i.e. aquifer dimension etc. (see Sec. 3.1). Within this study density dependent effects in two-phase flow are studied, i.e density differences between CO_2 and brine. Altmark is based on corresponding site data, i.e. geological stratigraphy etc. (see Sec. 3.2). This case study is dedicated to the scenario if CO_2 is injected in a gaseous state into a depleted gas reservoir. Therefore we deal with non-isothermal compressible flow. Stuttgart and Svalbard can be called as community benchmarks. These examples have been developed and discussed during two workshops in Stuttgart and Svalbard, respectively. In principal, they deal with 3-D two-phase flow. Finally we present the first H^2M example regarding to two-phase flow consolidation processes. We study the interaction of fluid flow and mechanical deformation during CO_2 injection.

Table 3
Benchmarks by sites and scenarios.

Problem type	Process type	Dimension	Doc
Ketzin	H^2	2-D(r)	Sec. 3.1
Altmark	THC^2	2-D(r)	Sec. 3.2
Svalbard	H^2/M	2-D	Sec. 3.3, [3]
Stuttgart	H^2	3-D	Sec. 3.4, [2]
Shear slip	H^2M	2-D	see TV III.2.2-1, this report

3 Results

3.1 Ketzin benchmark

We consider CO_2 injection into a sedimentary formation filled with brine (saline aquifer). We are interested in the near field two-phase flow and consolidation processes close to the well. Therefore the conceptual model for this application benchmark is a H^2M process model with axial symmetry. Fig. 1 depicts the benchmark sketch. The theoretical background is described in TV III.2.2-1 (this report).

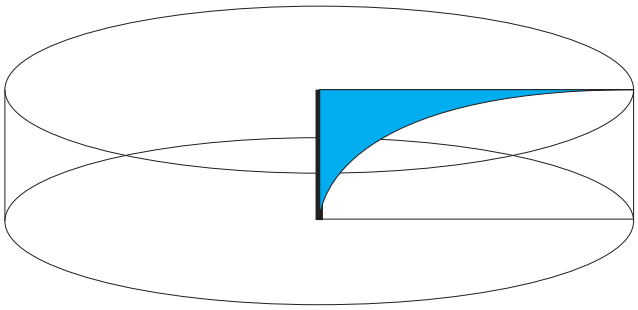

Fig. 1. Benchmark sketch.

The benchmark repository on the OGS site is at:
`https://geosys.ufz.de/trac/wiki/GFZ-InjectionWell`
`https://geosys.ufz.de/trac/browser/branches/Multiphase/H2M_Ketzin`

3.1.1 Benchmark definition: System geometry and conditions

- Geometry: The aquifer is at 770 m depth underneath the ground surface and it is bounded by parallel impermeable confining formations above and below. The aquifer thickness is very thin with 6 m only and it extends 200 m

in radial direction. The well radius is 0.2 m. An axial symmetric coordinate system is used.

- IC: The aquifer is located at a depth of 770 m under hydrostatic initial conditions. The saline aquifer is fully saturated with brine before injection starts. The reservoir temperature is assumed to be constant equal to 34°C. Initially, the stress tensor coefficients in the deep saline aquifer are assumed to be caused by the gravity force only, the distribution of which is calculated by solving the stress equilibrium with the volume force term $\rho \boldsymbol{g}$ (lithostatic conditions). This initial distribution analysis is used as the initial stress condition for modeling the CO_2 injection. For an overview about initial conditions see Tab. 4
- BC: We consider no flow conditions at the entire model domain boundary. Maximum water saturation and residual CO_2 saturation are assigned in the terms of Dirichlet boundary conditions at the domain boundary in the radial direction. On both top and bottom boundaries, the displacement in vertical direction is fixed. In the horizontal direction, displacement is fixed only on the outer boundary. The inner boundary is assumed to be free to move.
- ST: A vertical well is injecting CO_2 over the entire aquifer thicknes into the formation. The injection rate corresponds to a Neumann boundary condition of 0.4475×10^{-5} m/s.

Table 4
Initial conditions.

Term	Symbol	Value	Unit
CO_2 pressure	p^{CO_2}	0.01	MPa
Capillary pressure	p^c	6.5	MPa
Temperature	T	34	°C
Stresses	σ_{xx}	-6005191.5 + 7798.95 z	Pa
	σ_{yy}	-6005191.5 + 7798.95 z	Pa
	σ_{zz}	-20017305 + 25996.5 z	Pa

For details of the geometrical and boundary conditions see Fig. 2

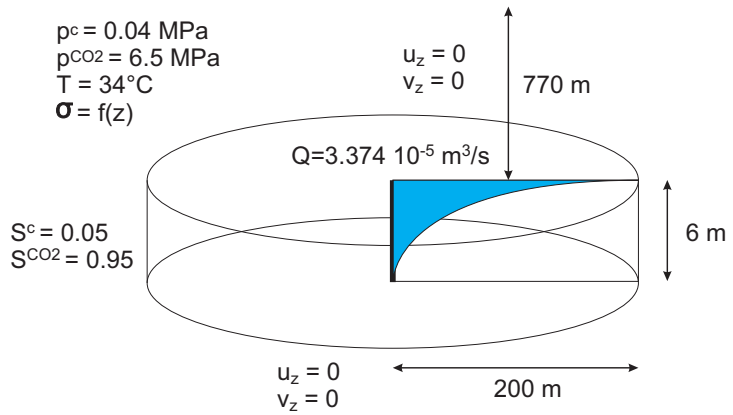

Fig. 2. System geometry and conditions.

3.1.2 Benchmark definition: System properties / parameters

System properties are material parameters of the porous medium as well as of fluid and solid phases. The material parameters are summarized in Table 5.

Table 5
Material properties.

Term	Symbol	Value	Unit
Porosity	n	0.26	–
Intrinsic permeability	k	3×10^{-13}	m^2
Brooks-Corey index		2	–
Entry pressure	p^D	10^4	Pa
Pore size distribution index	λ		–
Brine density	ρ^b	1173	$kg\cdot m^{-3}$
Brine viscosity	μ^b	1.252×10^{-3}	Pa·s
Residual brine saturation	S^b_{res}	0.35	–
Maximum brine saturation	S^b_{max}	0.95	–
CO_2 density	ρ^{CO_2}	848	$kg\cdot m^{-3}$
CO_2 viscosity	μ^{CO_2}	8.1×10^{-5}	Pa·s
Residual CO_2 saturation	$S^{CO_2}_{res}$	0.05	–
Maximum CO_2 saturation	$S^{CO_2}_{max}$	0.65	–
Young's modulus	E	2×10^{11}	Pa
Poisson's ratio	ν	0.3	–

- Formation properties: A homogeneous, isotropic aquifer is assumed with 26% porosity and 3×10^{-13} m^2 intrinsic permeability. The formation is deformable but with no fractures.
- Fluid properties: are kept constant in this study. We consider saturated brine (maximum salt concentration), CO_2 is in supercritical state under the present conditions.
- Two-phase flow functions: Liquid and solid phase densities are assumed to be constant. The Brooks-Corey's model is employed to characterize the hydraulic properties of liquid CO_2 and brine.

$$p^c = p^{CO_2} - p^b = p^D S_{eff}^{-(1/\lambda)} \tag{1}$$

$$k^b_{rel} = S_{eff}^{(2+3\lambda)/\lambda} \tag{2}$$

$$k^{CO_2}_{rel} = (1 - S^2_{eff})\left(1 - S_{eff}^{(2+\lambda)/\lambda}\right) \tag{3}$$

- Mineralogy: Brine and CO_2 are assumed to be in equilibrium with the rock (no chemical fluid-rock interactions considered so far).

- Rock mechanics: We consider poro-elasticity with constant parameters (Young's modulus and Poisson's ratio).

3.1.3 Benchmark definition: Numerical model

We use the finite element method for discretization. The coupling scheme is hybrid: the two-phase flow is solved monolithically, the deformation problem is solved after the flow step. Taking the injection well's radius as 0.2 m and cutting the 3D domain at the radius of 200 m, we generate a finite mesh for axisymmetrical analysis as depicted in Fig. 3.

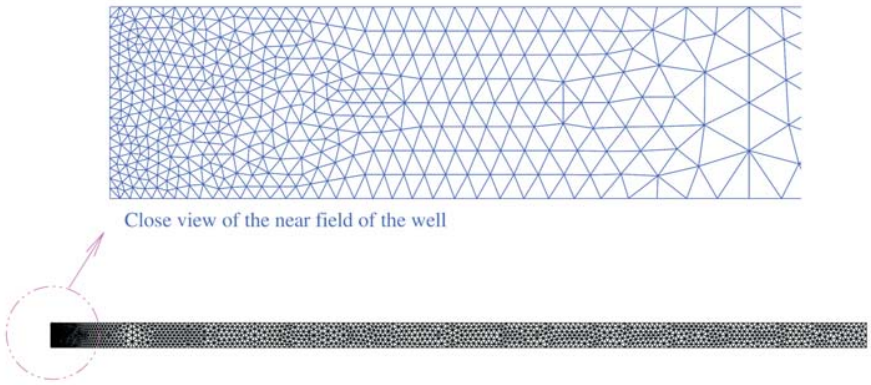

Fig. 3. Triangular mesh for finite element analyses.

3.1.4 Benchmark questions

We are interested in the following issues:

- Are density dependent effects important ?
- Will deformation processes influence the CO_2 injection process ?
- (Comparison of *pp* and *pS* schemes)
- (Code comparison OGS / TOUGH-FLAC)

In order to investigate the impact of solid deformation on the hydraulic field, the simulations of the two-phase flow process in the deep saline aquifer were performed considering and neglecting the coupled deformation process, respectively. To demonstrate this impact, in Fig. 4 the change of CO_2 saturation during a period of 1000 hours at two specified observation points is plotted, which are at a distance of 20 m and 50 m from the injection well, respectively.

Fig. 4 portrays that the propagation of CO_2 is slightly enhanced by deformation. On the other hand, the stress field is significantly altered by the CO_2 injection pressure in the near field. We can clearly see stress changes at the two observation points as depicted in Fig. 5. The tangential stress decreases

at the beginning of the injection due to the extension at the well surface, and then increases due to the propagation of the injection pressure. Since we assume that the initial stress is induced by the gravitational force exclusively, the initial stress distribution in the analyzed domain has a vertical gradient.

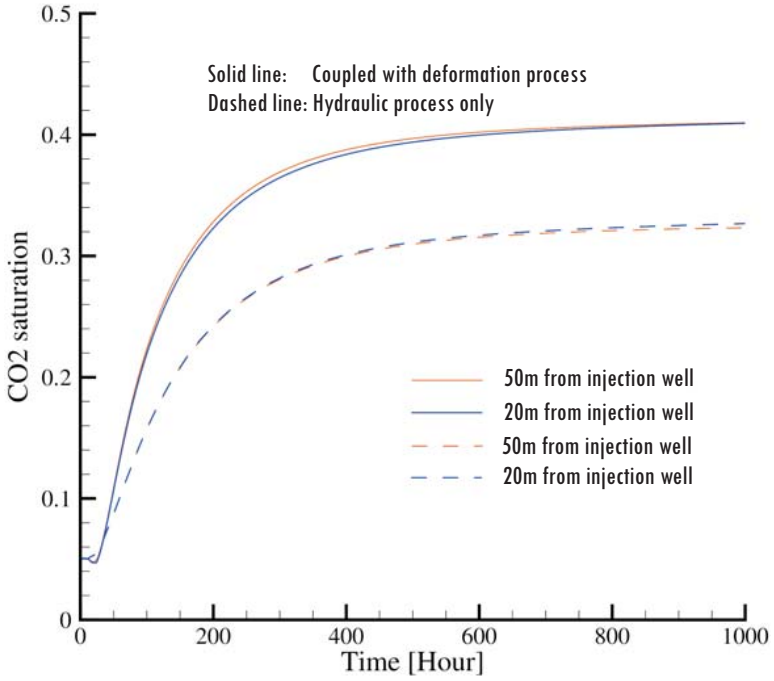

Fig. 4. Temporal evolution of CO_2 saturation in two observation points.

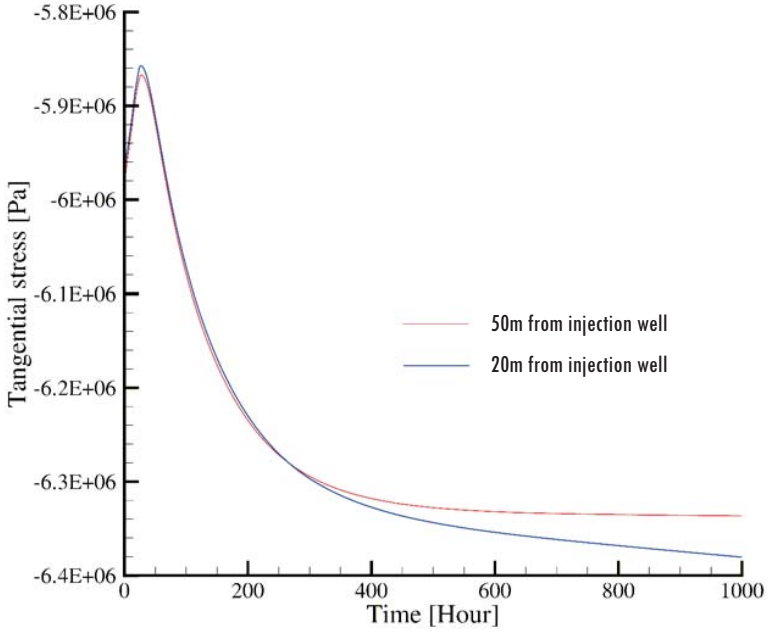

Fig. 5. Temporal evolution of tangential stresses in two observation points.

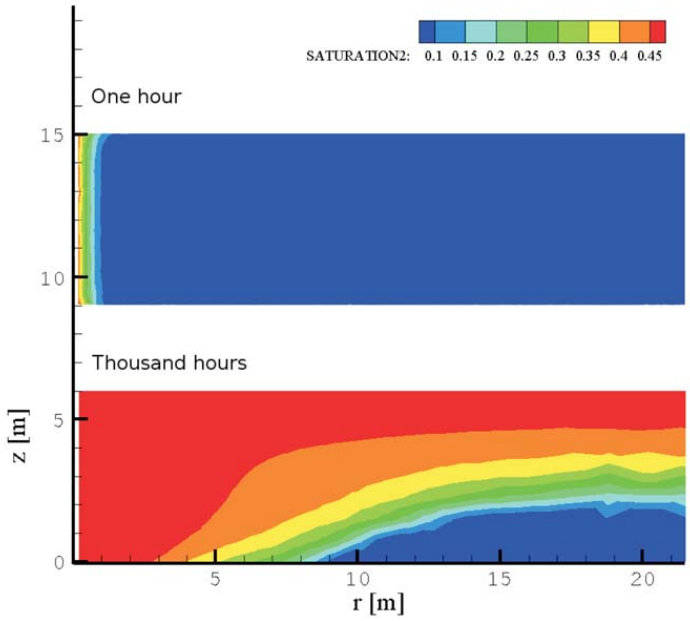

Fig. 6. Spatial distribution of the CO_2 saturation 1 and 1000 hours respectively after injection started.

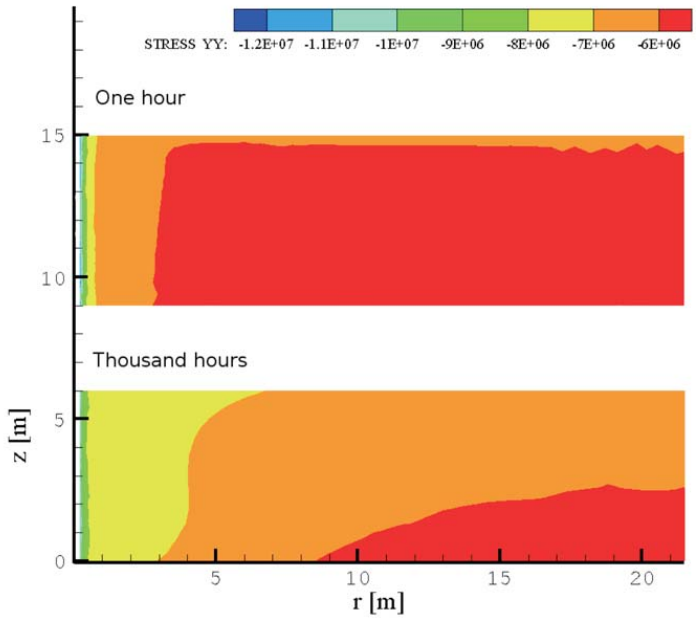

Fig. 7. Spatial distribution of tangential stresses 1 and 1000 hours respectively after injection started.

Due to the injection pressure of CO_2, the stress in the tangential direction increases significantly. Fig. 6 shows the distribution of the tangential stress near the injection well at the time of one hour and one thousand hours after the beginning of the injection.

Corresponding to the stress field demonstrated in Fig. 6, the distribution of carbon dioxide in the vicinity of the injection well at the same time is provided in Fig. 7. Comparing Fig. 6 and Fig. 7, we see that the distribution patterns of tangential stress and CO_2 are quite similar. This implies the coupling effect between hydraulic and mechanical processes.

3.2 Altmark benchmark

We consider multi-layered caprock-reservoir model for Altensalzwedel test. Here, entire layer is composed of four different rock types. Work is modeled for non-isothermal gas flow through different porous layers on injection of gaseous carbon dioxide under axisymmetric conditions. We do not consider gravity effects where gas is composed of three pure gaseous species, i.e. initially reservoir has been filled completely with methane and nitrogen then carbon dioxide has been introduced through injection well. In the mass transport, concentration distribution of each species has been calculated along with gas flow and heat transport. Fig. 8 shows the model configuration.

The benchmark repository on the OGS site is at:
`https://geosys.ufz.de/trac/wiki/GFZ-InjectionWell`
`https://geosys.ufz.de/trac/browser/branches/altmark`

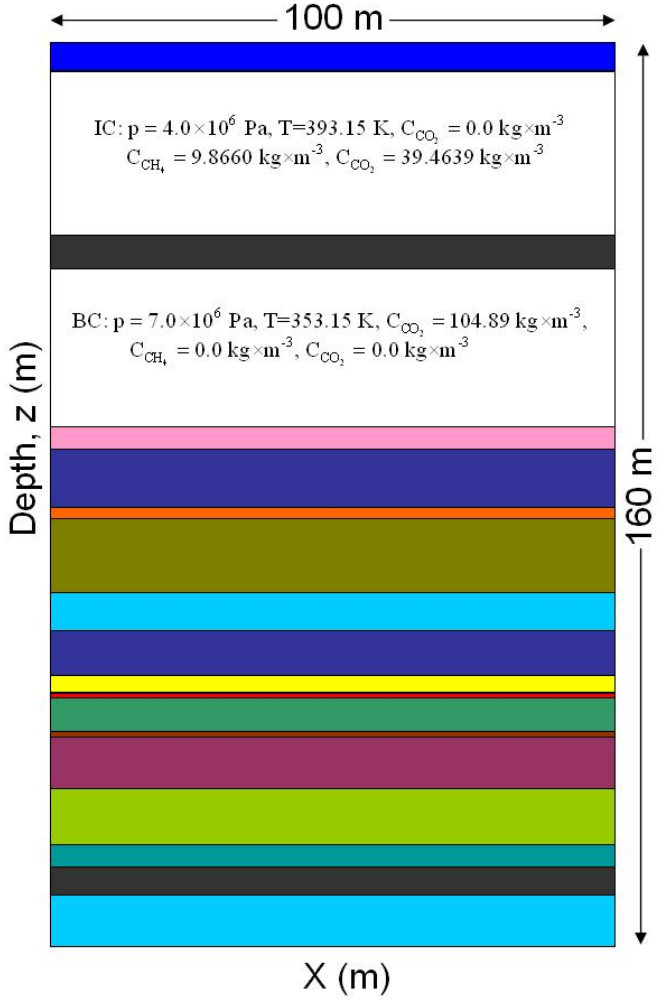

Fig. 8. System geometry and conditions.

3.2.1 Benchmark definition: System geometry and conditions

- Geometry: We have considered 19 main layers, whereas the top and bottom surfaces are located at depth of -3295 m and -3455 m. Observation well is 100 m far from the injection well. Since we consider axisymmetry, twodimensional model domain is taken in x-z plane, i.e. 160 m thick in z-direction and 100 m long in (radial) x-direction.
- IC: We assume that caprock-reservoir is filled with 20% methane and 80% nitrogen at pressure of $4.0{\cdot}10^6$ Pa and temperature 120°C. We have estimated the effective molecular weight of this gaseous mixture by $M_{\text{eff}} = \sum \omega_i, M_i$. Following, using the molecular weights and mole-fractions of each pure gas component at initial pressure and temperature, we found that the effective molecular weight is 40.0129 kg·kmol^{-1}. Hence, density of the gas is 48.9632 kg·m^{-3}. With this information we assigned initial component concentrations of $C_{CO_2} = 0$ kg·m^{-3}, $C_{CH_4} = 9.8660$ kg·m^{-3} and $C_{N_2} = 39.4639$ kg·m^{-3}.
- BC: We are injecting CO_2 through injection well with $7.0{\cdot}10^6$ Pa pressure and 80°C temperature which is lower than the initial temperature of the reservoir. Since the injected gas consists of 100% carbon dioxide, with no methane and no nitrogen, the density of the injected gas is 104.8974 kg·m^{-3}. Consequently, the concentrations of components in the injected gas are $C_{CO_2} = 104.8974$ kg·m^{-3}, $C_{CH_4} = 0$ kg·m^{-3} and $C_{N_2} = 0$ kg·m^{-3}.

3.2.2 Benchmark definition: System properties / parameters

Model parameters are the physical and thermodynamical properties of the gaseous mixture and the solid, along with medium properties of the porous media.

- Medium properties: Layers of the caprock-reservoir are composed of four different types of rocks, for example: Anhydrite, Silicate, Sandstone, and Siltstone. The layers have different porosity and density ranging from 0.001 to 0.172 and $2.18{\cdot}10^3$ kg·m^{-3} to $2.94{\cdot}10^3$ kg·m^{-3}, respectively. Based on the porosity value each layer has different permeability. All this information has been summarized in Tab. 6.
- Fluid properties: In the present study certain material parameters of the solid and the gaseous mixture are constant which is mentioned in Tab. 7.

Table 6
Medium properties of the multilayered caprock-reservoir.

No.	**Depth (m)**	**Rock type**	z_p **(m)**	**n**	$\mathbb{K}$ **(m^2)**	ρ^s **(kg· m^{-3})**
6	3295-3300	Sandstone	5	0.039	2.2731e-016	2 460
7	3295-3329	Anhydrite	29	0.010	3.0900e-019	2 940
8	3329-3335	Sandstone	6	0.046	5.0621e-016	2 940
9	3335-3363	Siltstone	28	0.011	4.9058e-019	2 700
10	3363-3367	Sandstone	4	0.058	1.5581e-015	2 940
11	3367-3378	Siltstone	11	0.011	4.9058e-019	2 700
12	3378-3380	Sandstone	2	0.025	2.6301e-017	2 940
13	3380-3392	Siltstone	12	0.011	4.9058e-019	2 700
14	3392-3398	Sandstone	6	0.073	4.7542e-015	2 940
15	3398-3406	Siltstone	8	0.011	4.9058e-019	2 700
16	3406-3409	Sandstone	3	0.162	2.2704e-013	2 940
17	3409-3410	Siltstone	1	0.011	4.9058e-019	2 700
18	3410-3416	Sandstone	6	0.154	1.7760e-013	2 940
19	3416-3417	Siltstone	1	0.011	4.9058e-019	2 700
20	3417-3426	Sandstone	9	0.172	3.0358e-013	2 940
21	3426-3436	Claystone	10	0.011	4.9058e-019	2 700
22	3436-3440	Sandstone	4	0.082	8.3552e-015	2 940
23	3440-3446	Claystone	6	0.011	4.9058e-019	2 720
24	3446-3455	Sandstone	9	0.023	1.7552e-017	2 940

Table 7
Material parameters of solid and gas.

Meaning	**Symbol**	**Value/ Ref.**	**Unit**
Density	ρ^g	$\frac{M_{\text{eff}} p}{zRT}$	kg·m^{-3}
Dynamic viscosity	μ^g	$1.78{\cdot}10^{-5}$	Pa·s
Heat capacity	c_p^g, c_p^s	$4.28{\cdot}10^3$, $1.091{\cdot}10^3$	J·kg^{-1}·K^{-1}
Thermal conductivity	κ^g, κ^s	0.60, 0.41	W·m^{-1}·K^{-1}
Diffusion coefficient	$D^o_{CO_2,CH_4,N_2}$	$0.965{\cdot}10^{-5}$, $2.0{\cdot}10^{-5}$, $1.78{\cdot}10^{-5}$	m·s^{-1}
Dispersivity	α_L, α_T	$1.0{\cdot}10^{-4}$, $1.0{\cdot}10^{-3}$	m

3.2.3 Benchmark definition: Numerical model

We use the finite element method for discretization of the governing equations. The problem is analyzed on a 19 000 quad type mesh up to time duration 1 000 s on a twodimensional domain in the x-z plane. Here a constant step size (Δx) has been taken in x-direction and in z-direction we used variable step size (Δz) depending on the thickness of the rock layer, i.e. thin layers have smaller Δz than thick layers. A staggered coupling scheme has been employed, i.e. the gas flow process is solved first then the heat transport problem, and finally the mass transport equations.

3.2.4 Benchmark questions

We are interested in gas flow coupled with heat and mass transport processes. Here, we consider temperature and concentration effects on the gas flow through ideal gas law. Since we are using pressure over 20 Pa, a compressibility factor is important to introduce. Temperature effect is directly through ideal gas law, but concentration effect comes through effective molecular weight of the gaseous mixture; which is the sum of mass fraction times species molecular weight.

In Fig. 9 we have presented the time-evolution of the gas pressure, temperature and concentrations of each species (i.e., C_{CO_2}, C_{CH_4}, C_{N_2}) at two observation point in the reservoir at time $t = 1\,000$ s. The observation points are placed at the depth of -3437.5 m, one of them is located in a distance of 5.0 m from the injection well, and the second is 10.0 m away. We have neglected all source/sink terms in the present calculation. As we assume that gaseous mixture is compressible hence, transient flow is developing. In the Table 6, we have presented medium properties of different layers of the caprock. Due to variation in permeability ($\mathbb{K}$) flow is not uniform, i.e. fast flow in the layer which have high permeability and slow/no flow in the layer with very low permeability. In the layer with higher permeability, advective heat and mass transport is dominated whereas in layers with very low permeability heat and mass transport are mainly due to diffusion processes.

In Figs. 10-11 we present the distribution of gas pressure, temperature, density and concentration of each species of the gas mixture in the reservoir at time $t = 1\,000$ s. Fig. 10 shows that after $t = 1\,000$ s in the layer with largest permeability (i.e., $3.0358{\cdot}10^{-13}$ m^2) a $4.2011{\cdot}10^6$ Pa pressure; 84.0800 kg·m^{-3} CO_2 concentration; 2.5740 kg·m^{-3} CH_4 concentration; 10.0294 kg·m^{-3} N_2 concentration isolines have been reached about 63.0885 m.

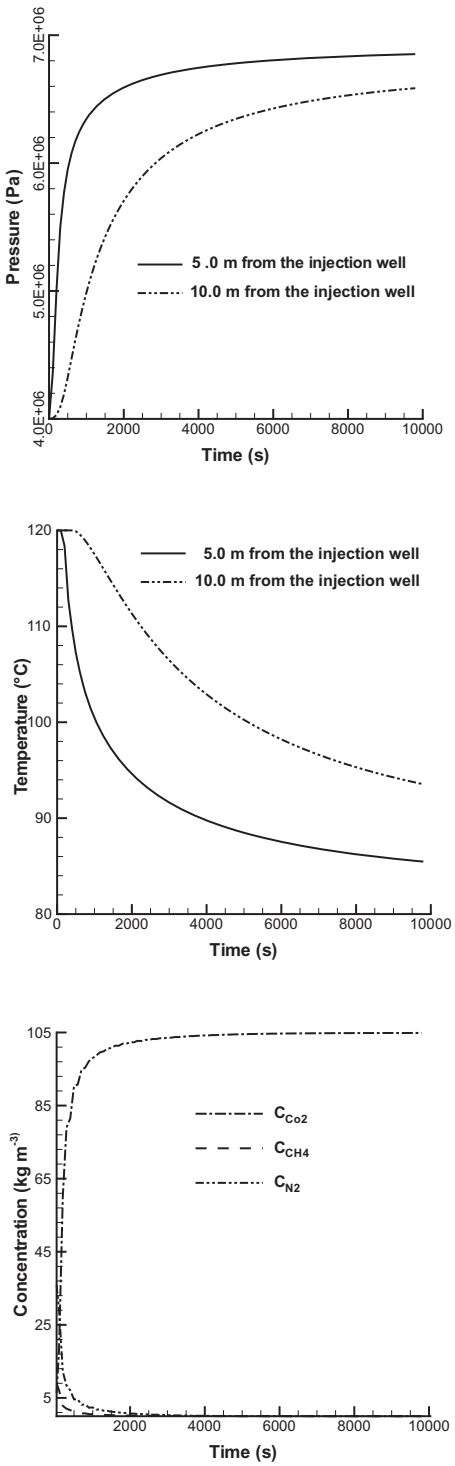

Fig. 9. Temporal evolution of the gas pressure as well as the gas temperature at two observation points, and temporal evolution of the concentration of each species at an observation point 5 m away from the injection well.

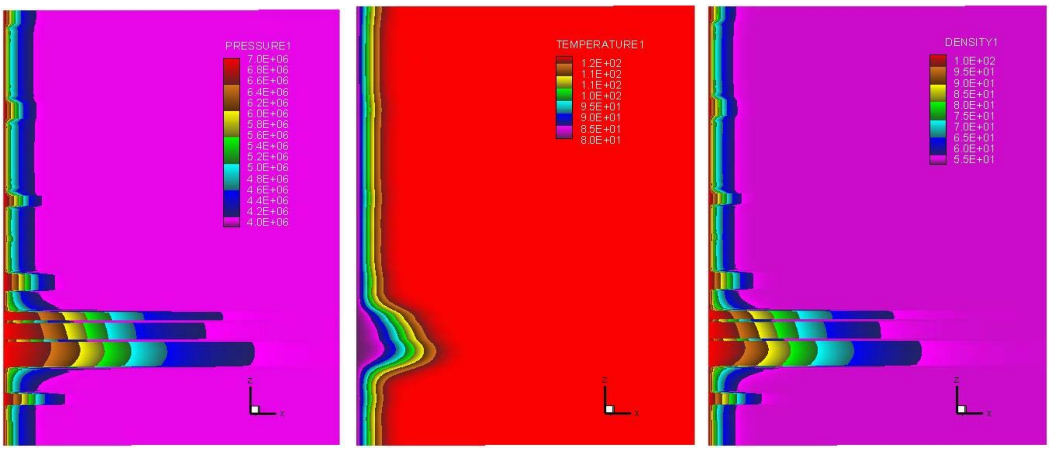

Fig. 10. Distribution of the gas pressure, temperature and density at $t = 1\,000$ days.

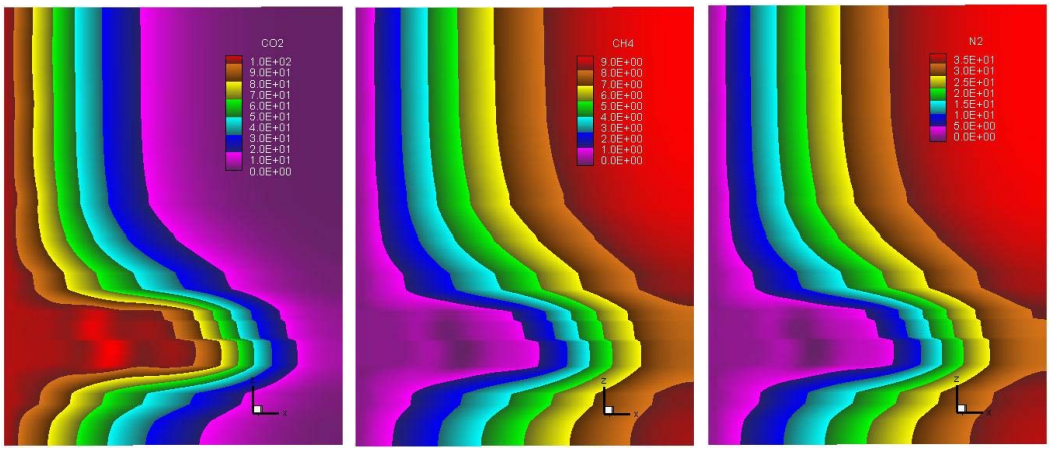

Fig. 11. Distribution of the species concentration in the gas at $t = 1\,000$ days.

3.3 Svalbard benchmark

Svalbard benchmark (cf. [3] is defined to answer questions regarding the ultimate fate of the injected CO_2 plume. The purpose of the benchmark aims to achieve an assessment of upscaling and modeling applicable for the CO_2 storage problem and some indication of the uncertainty introduced during the stage of model adaption. With these two purposes, the benchmark is idealized in a domain and fluid properties in a hope to isolate model uncertainty.

3.3.1 Benchmark definition: System geometry and conditions

- Geometry: The aquifer with dip of 1% is bounded by parallel impermeable confining formation above and below. The thickness of the aquifer is 50 m, the length in the dip direction is 200 km, and the width is 100 km in the direction perpendicular to dip.
- IC: The center of the aquifer is situated at a depth of 2.5 km below the water table, under hydrostatic and geothermal conditions based on a surface temperature of 10°C and a geothermal gradient of 25°C/km.
- BC: The flow boundary conditions in the horizontal directions are constant head, and fixed temperature boundary conditions are applied at the boundary of the domain.
- ST: A horizontal well, injecting at the bottom impermeable boundary of the formation, placed 50 km updip from the lowest point of the formation, and in the center with respect to the horizontal direction perpendicular to dip. The well length is 1 km, and the orientation is perpendicular to the dip of the formation. Injection rate is 1 Mt/year for 20 years. Infinite post-injection time period.

3.3.2 Benchmark definition: System properties / parameters

- Homogeneous aquifer permeability of 10-13 m^2, porosity of 15%. Rock thermal conductivity of 3 W/(m·K). The formation is incompressible, with no fractures.
- Based on typical PTV data. Pure brine, no salt concentration.
- Primary drainage relative permeability for water and for CO_2 by simple power law expressions (Brooks and Corey), given respectively by

$$k_{r,w} = S_{w,n}^4 \tag{4}$$

$$k_{r,\mathrm{CO_2}} = 0.4 \left(1 - S_{w,n}^2\right) \left(1 - S_{w,n}\right)^2 \tag{5}$$

where $S_{w,n}$ is the normalized water saturation where the irreducible water saturation is set to $S_{w,cr} = 0.2$. The primary drainage capillary pressure

(units bar) is given by

$$p_{c,d} = 0.2\, S_{w,n}^{-1/2} \tag{6}$$

- Hysteresis may be included in both relative permeability and capillary pressure description. Irreducible CO_2 saturation for the bounding imbibition curve (imbibition from irreducible water saturation) is assigned the value $S_{CO_2,cr} = 0.2$.
- If study of mineral reactions is desired, standard Berea sandstone is recommended with the brine in equilibrium with the rock initially.
- If geomechanical effects are interested, overburden properties are consistent with the initial conditions and geomechanical properties of the aquifer are consistent with Berea sandstone.

3.3.3 Benchmark definition: Numerical model

We use the $p_w S_n$ and $p_c p_{nw}$ models to simulate for the 2D domain upscaled from the original 3D problem of the definition with no thermal effect and the adjusted fluid properties: CO_2 density 479 kg/m^3, brine density 1045 kg/m^3 and CO_2 viscosity $3.95{\cdot}10^{-5}$ Pa·s, brine viscosity $2.535{\cdot}10^{-4}$ Pa·s.

The assumptions made for the scale-up are:

- Averaged over the perpendicular line to the aquifer orientation.
- No dissolution and convective mixing of brine water.
- No mineralization.

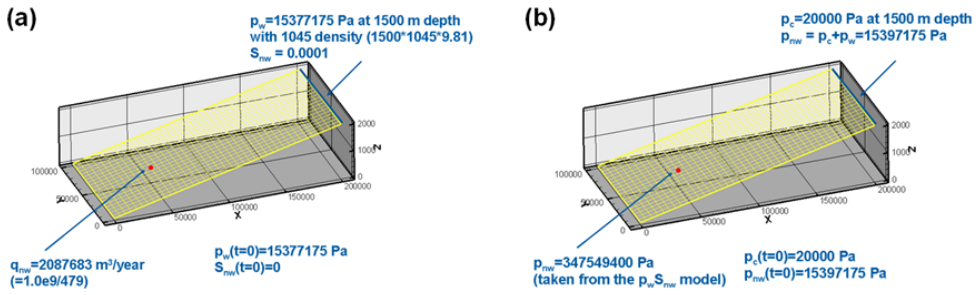

Fig. 12. Boundary conditions for (a) the $p_w S_n$ model and (b) the $p_c p_{nw}$ model.

3.3.4 OGS results

Based on the assumptions made in the 2D grid, the resulting pressure and CO_2 saturation obtained from both methods are depicted in Fig. 13 and 14. Both results for this simulation period of 100 years are in good agreement. Pressure change between 20 years and 100 years are minimal indicating that much longer time (several orders bigger time scales) is needed to immobilize

the injected CO_2 by CO_2 residual saturation. However, the simulation is not extended that long after observing little difference of pressure change.

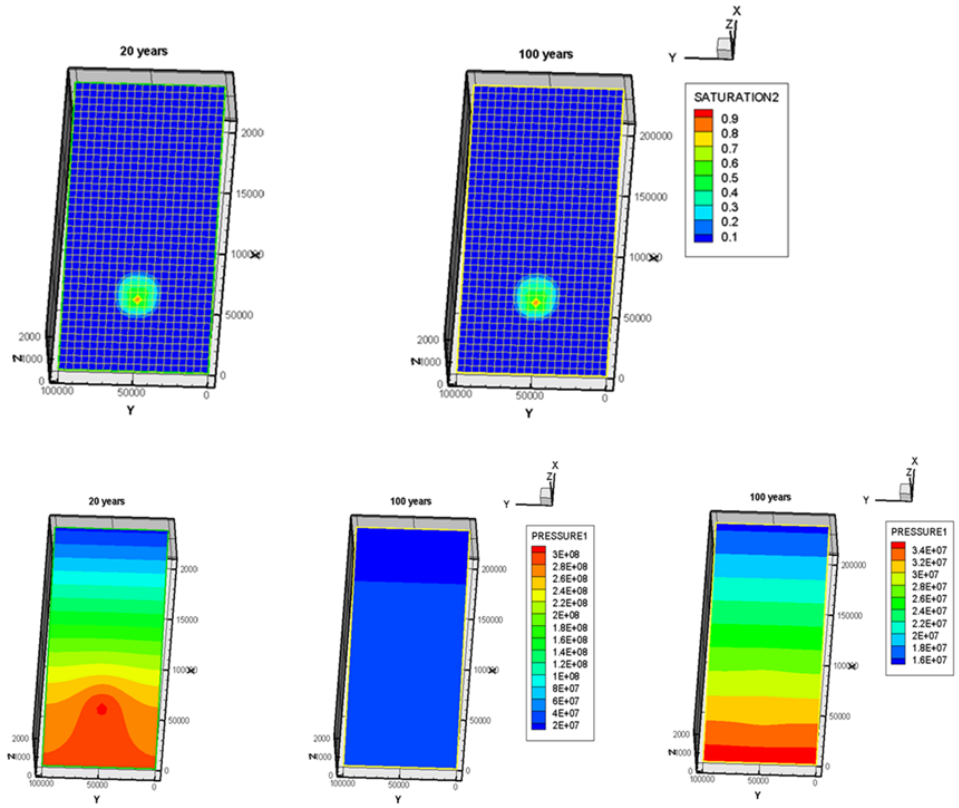

Fig. 13. Pressure and CO_2 saturation at 20 and 100 years obtained from the $p_w S_n$ model.

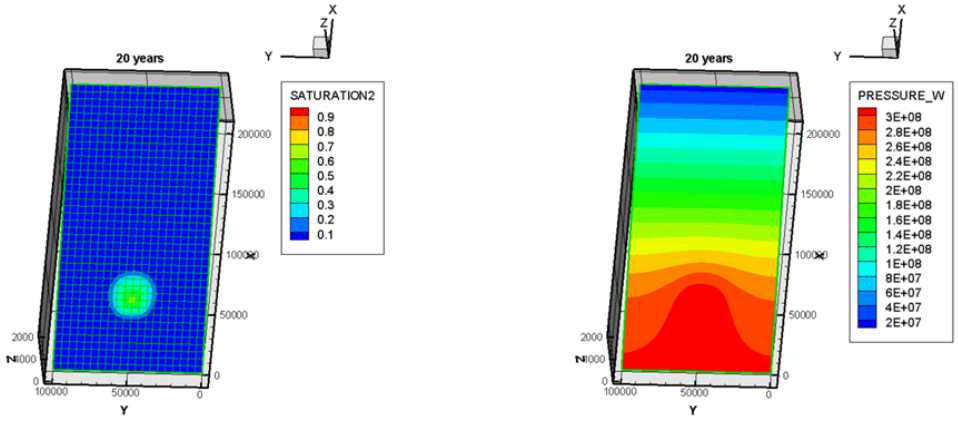

Fig. 14. Pressure and CO_2 saturation at 20 years obtained from the $p_c p_{nw}$ model.

3.4 Stuttgart benchmark

Three problem-oriented benchmark tests have been defined by the Stuttgart/Bergen (Norway) teams. The benchmarks definitions have been devloped and presented during a workshop in Stuttgart in 2008, therefore, we refer to them as the Stuttgart benchmarks in the CO_2 systematic. The definitions as well as the results of the Stuttgart benchmark studies are recently published in [2].

The benchmark definitions are available at
`http://www.hydrosys.uni-stuttgart.de/co2-workshop`.

3.4.1 CO_2 Plume evolution and leakage through an abandoned well

The first Stuttgart benchmark is dealing with CO_2 injection into a deep saline aquifer and CO_2 migrating within the formation. After reaching the leaky well the CO_2 rises up to a shallower aquifer. The goal of the benchmark study is the quantification of possible the leakage rate which depends on the pressure build-up in the aquifer due to CO_2 injection. The leckage scenario is shown in Fig 15. This test case is dedicated for risk assessement of CO_2 storage. The test case is 3D and two-phase flow (H^2 processes, liquid/liquid system) is considered.

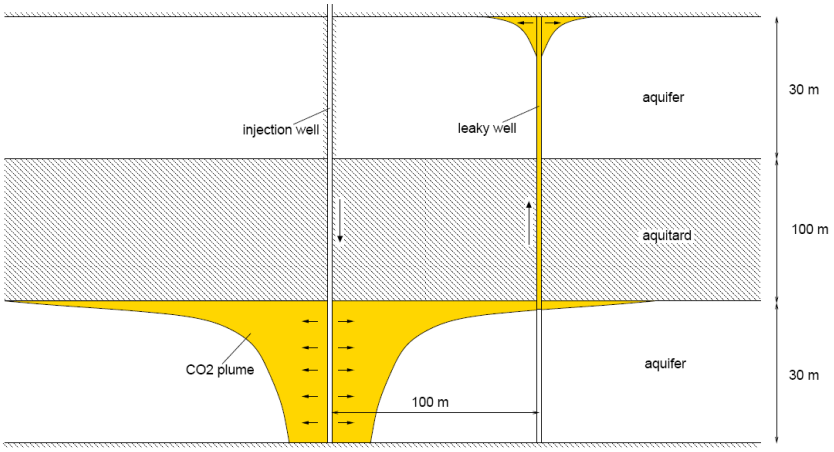

Fig. 15. Leakage scenario, from [2]

Fig. 16 shows first qualitative results of the 3-D two-phase (H^2) simulations with OGS. Liquid pressure and saturation of CO_2 are plotted for a selected time. The plots show the radial propagation of the carbon dioxide. We see the density effect of upcoming CO_2 due to the smaller density in comparison to the saline water. The carbon dioxide reaches the leaky well after about 100 days.

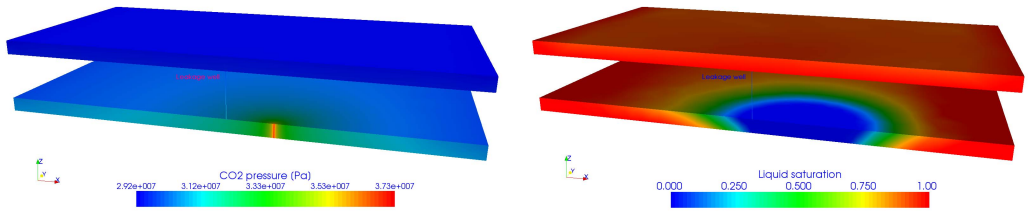

Fig. 16. Results of the 3-D two-phase flow simulation: phase pressure (left) and saturation (right) of CO_2

More information about the ongoing work is available at:
`https://geosys.ufz.de/trac/wiki/TheBenchmarkForCO2WorkshopInStuttgart`

3.4.2 Enhanced CH_4 recovery in combination with CO_2 storage in depleted gas reservoirs

The second Stuttgart benchmark case is based on the classic five-spot problem. The test problem is used for the numerical simulation of generic enhanced gas recovery scenarios. Fig. 17 shows a schematic of the five-spot problem with an injection well at the centre and production wells at the corners. Due to symmetry, only a quarter of the domain has to be modelled.

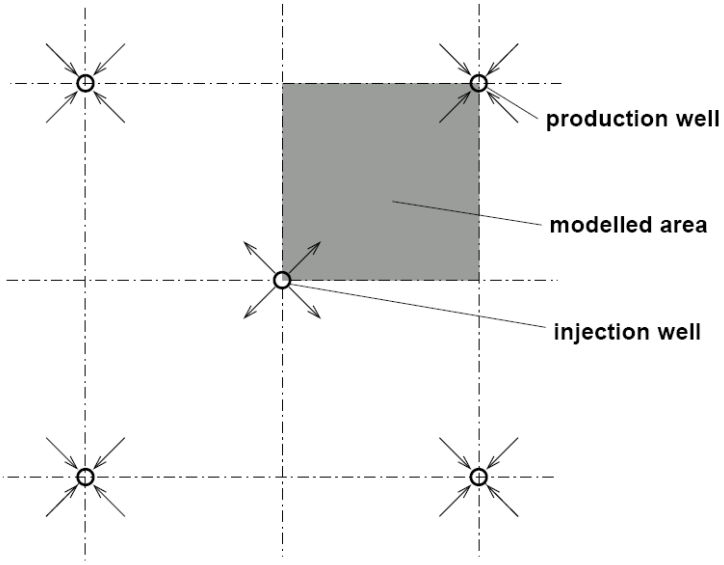

Fig. 17. Five-spot pattern depicting the CO_2 injection well and the CH_4 production wells, from [2]

3.4.3 Estimation of the CO_2 storage capacity of a geological formation

The third Stuttgart benchmark is based on a real site, the Johansen formation off the coast of Norway (Fig. 18). The model domain contains a fault zone. The injection well is located near the fault. The first goal of this benchmark study is to determine the amount of CO_2 which can be safely stored in the formation. Secondly, the trapping mechanisms are studied, i.e. ratio between dissolved CO_2 in water and CO_2 still in phase. Moreover hysteresis effects of the CO_2 relative permeability-saturation relationships are considered.

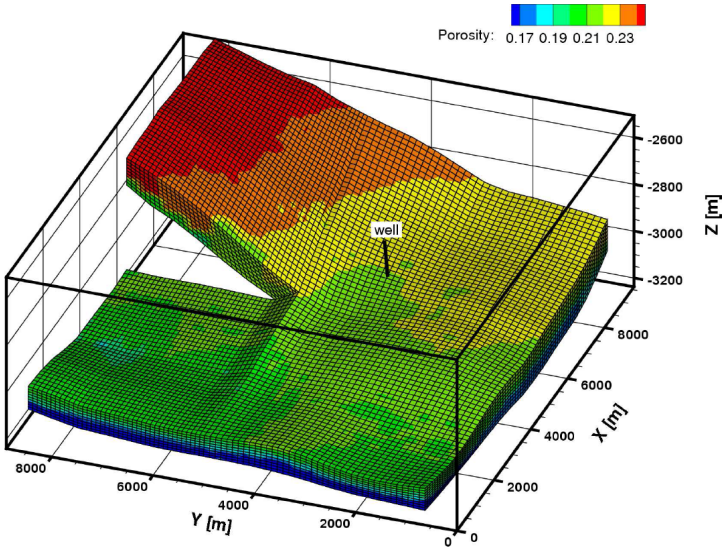

Fig. 18. Johansen formation off the coast of Norway, porosity distribution, from [2]

4 Summary and Discussions

Benchmarking using examples which are relevant for the processes during CO_2 injection and storage is an important cross-cutting project part for the validation of numerical methods and for code comparison. Specific process-related benchmarks were defined for partial processes and selected coupling scenarios of the overall THMC process. Typical site-specific benchmarks were chosen from literature and defined from the first project results, respectively.

5 Outlook

The proposed benchmarks will be discussed on the next modellers meeting in March 2010. Based on this, the comparison of the various codes which are used from the project partners should be performed to define their capabilities

and limitations. Site-specific benchmarks serve as the basis for the definition of site-related scenarios for the Altensalzwedel area.

References

[1] Centler F., Shao H., de Biase C., Park C.-H., Regnier P., Kolditz O., Thullner M. (2009) GeoSysBRNS – A flexible multidimensional reactive transport model for simulating biogeochemical subsurface processes, *Comput. Geosci.*, doi:10.1016/j.cageo.2009.06.009 (in print).

[2] Class H., Ebigbo A., Helmig R., Dahle H.K., Nordbotten J.M., Celia, M.A., Audigane P., Darcis M., Ennis-King J., Fan Y., Flemisch B., Gasda S.E., Jin M., Krug St., Labregere D., Beni A.N., Pawar R.J., Sbai A., Thomas S.G., Trenty L., Wei, L. (2009) A benchmark study on problems related to CO_2 storage in geologic formations: Summary and discussion of the results, *Comput. Geosci.*, doi:10.1007/s10596-009-9146-x (in print).

[3] Dahle H.K., Eigestad G.T., Nordbotten J.M., Pruess K. (2009) A model-oriented benchmark problem for CO_2 storage, *Technical Report*, Svalbard (available at `http://org.uib.no/cipr/Workshop/2009/CO2`).

[4] Kolditz O., Shao H. (Eds.) (2010) OpenGeoSys – Developer Benchmark Book, *Technical Report UFZ and BGR*, Version 4.10.07, Leipzig.

[5] Shao H., Dmytrieva S., Kolditz O., Kulik D., Pfingsten W., Kosakowski G. (2009) Modeling reactive transport in non-ideal aqueous-solid solution systems, *Appl. Geochem.* **24**, 12871300.

[6] Shao H., Kulik D.A., Berner U., Kosakowski G., Kolditz O. (2009) Modeling the competition between solid solution formation and cation exchange on the retardation of aqueous radium in an idealized bentonite column, *Geochem. J.* **43**, e37e42.